

Theoretical and experimental analysis of AlGaN_xP micro-LED array with square-circle anode

Chao Tian, Weibiao Wang, Jingqiu Liang, Zhongzhu Liang, Yuxin Qin, and Jinguang Lv

Citation: AIP Advances **5**, 041309 (2015); doi: 10.1063/1.4904217

View online: <http://dx.doi.org/10.1063/1.4904217>

View Table of Contents: <http://aip.scitation.org/toc/adv/5/4>

Published by the American Institute of Physics

Articles you may be interested in

Heat dissipation analysis of bendable AlGaN_xP micro-LED arrays

AIP Advances **7**, 015209 (2017); 10.1063/1.4975225

GaN micro-light-emitting diode arrays with monolithically integrated sapphire microlenses

Applied Physics Letters **84**, 2253 (2004); 10.1063/1.1690876

III-Nitride full-scale high-resolution microdisplays

Applied Physics Letters **99**, 031116 (2011); 10.1063/1.3615679

Growth of monolithic full-color GaN-based LED with intermediate carrier blocking layers

AIP Advances **6**, 075316 (2016); 10.1063/1.4959897

Characteristics and applications of micro-pixelated GaN-based light emitting diodes on Si substrates

Journal of Applied Physics **115**, 033112 (2014); 10.1063/1.4862298

Size-dependent efficiency and efficiency droop of blue InGaN micro-light emitting diodes

Applied Physics Letters **101**, 231110 (2012); 10.1063/1.4769835



Theoretical and experimental analysis of AlGaInP micro-LED array with square-circle anode

Chao Tian,^{1,2} Weibiao Wang,^{1,a} Jingqiu Liang,^{1,b} Zhongzhu Liang,¹
Yuxin Qin,¹ and Jinguang Lv¹

¹*State Key Laboratory of Applied Optics, Changchun Institute of Optics, Fine Mechanics and Physics, Chinese Academy of Sciences, Changchun, Jilin 130033, China*

²*University of Chinese Academy of Sciences, Beijing 100049, China*

(Received 11 October 2014; accepted 24 November 2014; published online 10 December 2014)

An array of 320×240 micro-light-emitting diodes (micro-LEDs) based on an AlGaInP epitaxial wafer and with a unit size of 100 μm×100 μm was designed and fabricated. The optimum width of the isolation groove between adjacent light-emitting units was determined based on a compromise between full isolation of each LED and maximization of the light emitting area, and was found to be 20 μm. The grooves were filled with a mixed Si granule-polyurethane composite medium, because this type of insulating material can reflect part of the emitted light from the sidewall to the window layer in each light-emitting unit, and could thus improve lighting output efficiency. The 10-μm-wide square-circle anode was designed to increase the light emitting area while simultaneously being simple to fabricate. The device current used was in the 0.42–1.06 mA range to guarantee internal quantum efficiency of more than 85%, with a corresponding voltage range of 2–2.3 V. The layered temperature distribution in a single unit was simulated under a drive voltage of 2.2 V, and the maximum device temperature was 341 K. The micro-opto-electromechanical systems (MOEMS) technology-based fabrication process, experimental images of the device and device test results are presented here. © 2014 Author(s). All article content, except where otherwise noted, is licensed under a Creative Commons Attribution 3.0 Unported License. [<http://dx.doi.org/10.1063/1.4904217>]

INTRODUCTION

Micro-light-emitting diode (micro-LED) arrays that can be used as optical switches and microdisplays in communication networks have attracted considerable attention in recent years.^{1–4} Because of their micro-scale size and energy-saving characteristics, micro-LED arrays can offer better current distribution, higher brightness, more uniform light output and faster response times than regular illumination or display devices.^{5,6} Reliable AlGaInP-based LEDs with high brightness are attractive devices because AlGaInP has a direct energy bandgap in the visible spectrum in the yellow to red region. Recently, the performance of these devices improved significantly with progress in material growth methods, device and electrode designs, and fabrication technologies.^{7–10} However, array structures for vertical current-injection LEDs on a single wafer may provide more uniform current injection with a smaller package size when compared with a large-sized single LED. Array structure designs for monolithic LEDs are therefore required for high current operation. The thermal management of multiple LEDs is also important to enable good device reliability and high efficiency.^{11–13}

In this study, a micro-LED array based on an AlGaInP epitaxial wafer that was designed on the basis of a theoretical analysis is presented. The required width of the isolation groove between adjacent light-emitting units and the light extraction efficiency with Si-polyurethane (a silicon granule and

^aElectronic mail: wangwbcn@163.com

^bElectronic mail: liangjq@ciomp.ac.cn.

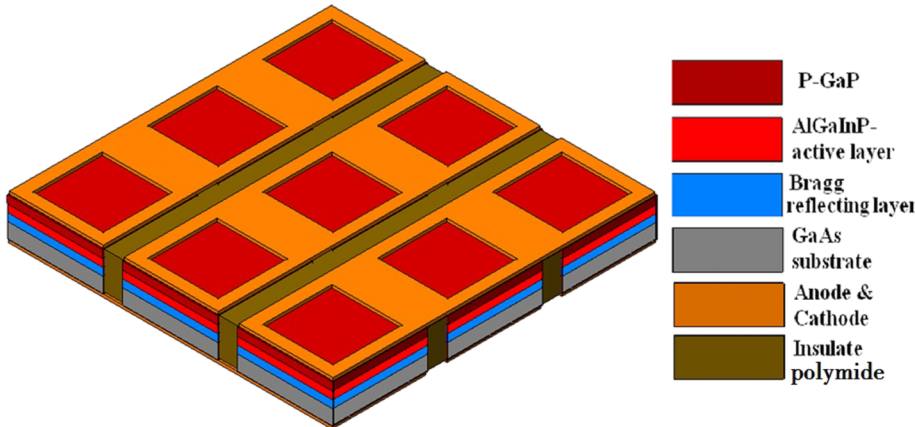


FIG. 1. Structure of the AlGaInP LED micro-array with the square-circle anode.

polyurethane multiple composite) filling the isolation groove are calculated. After simulation of the current and temperature distributions of a single unit with a square-circle anode, the appropriate anode width was confirmed. The fabrication process, which is based on micro-opto-electro-mechanical systems (MOEMS) technology, is then presented.

THEORETICAL ANALYSIS AND DESIGN

Because the AlGaInPlattice matches the GaAs substrate lattice well, the AlGaInP epitaxial multi-layers were grown on Si-doped n-GaAs substrates by metal-organic chemical vapor deposition. The epitaxial wafer included a Bragg reflector (DBR) layer, an AlGaInP quantum well active layer, a current spreading layer (p-GaP) and a contact layer (p+-GaP). The epitaxial wafer thickness was approximately 380 μm . The Bragg reflector layer consisted of a low reflectivity layer and a high reflectivity layer with an optical thickness of 1/4 of the emission wavelength. The DBR layer had an AlGaAs/AlAs structure, and was introduced to reflect light toward the substrate and back toward the upper surface to improve the light extraction efficiency.¹⁴

A schematic diagram of the AlGaInP LED micro-array with the square-circle anode is shown in Figure 1. Each unit consists of an isolation groove and a light-emitting region. Because the area of each unit region is constant, widening the isolation groove will reduce the light emitting area and thus will also reduce the light extraction efficiency. The isolation groove width must be determined based on a compromise between full isolation of each LED and an increase of the light emitting area. By taking the fact that the epitaxial layer thickness was approximately 15 μm and the need for the groove to be etched into the substrate to prevent crosstalk between different light emitting units into account, a groove depth of 20 μm was chosen. If we select the depth aspect ratio to be 1:1 with a groove width of 20 μm , then the area of the light emitting zone will be 80 $\mu\text{m} \times 80 \mu\text{m}$. By ignoring the shading effect of the electrode, the light extraction efficiency was calculated to be 64%. The insulating and opaque Si granule and polyurethane-based composite materials were used to fill the isolation groove. The Si-polyurethane composite could reflect part of the light from the sidewall toward the window layer in each light-emitting unit, and could thus improve the light extraction efficiency. In theory, a higher Si granule volume ratio guarantees higher reflectivity for the composite materials, and the light efficiency can also be more obviously improved; however, depending on the arrangement of the nanoparticles in the liquid, the highest volume ratio appeared in a six-angle dense stacking structure, at which point the specific concentration ratio of Si granules to polyurethane is 0.74.

The current distribution can affect the light emission efficiency and the working temperature of the micro-LED array greatly. The anode structure is also important for the device performance. Using the laser diode model proposed by Amann and Kappeler, simulations of the current density distribution of the LED array can be performed.¹⁵ Because the LED array in this study shows fine consistency, we need only calculate the current distribution for an individual unit. Figure 2 shows a

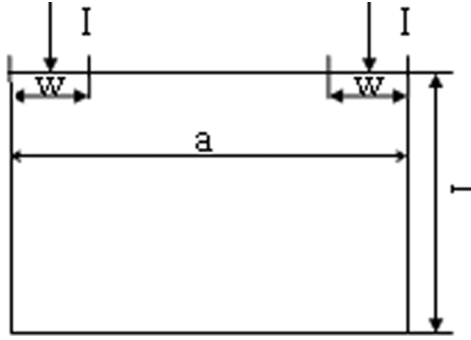


FIG. 2. Simplified current injection model.

simplified single unit structure. I , w , a and T represent the injection current intensity, the electrode width, the single unit width, and the current spreading layer thickness, respectively.

The ohmic contact resistivity between the semiconductor and the metal is represented by ρ_c , the resistivity of the p-GaP layer is represented by ρ and the p-GaP layer thickness is T . Usually, the contact resistance ρ_c is much less than $\rho_t/2$ and is thus negligible. $J(x)$ is the active layer transverse current density, which is given by Eq. (1):

$$J(x) = \frac{2}{\pi L} \sum_{i=1}^N \frac{I_i}{w_i} \arctan\left(\frac{\sinh(\pi w_i/4T)}{\cosh(\pi(x - x_i)/2T)}\right), \quad (1)$$

where L is the electrode length. In this model, L is also the length of the single unit LED in the array. Using the square-circle anode, Eq. (1) can be simplified to obtain

$$J(x) = \frac{I/2}{w} \left[\arctan\left(\frac{\sinh(\pi w/4T)}{\cosh(\pi(x - \frac{L-w/2}{2})/2T)}\right) + \arctan\left(\frac{\sinh(\pi w/4T)}{\cosh(\pi(x + \frac{L-w/2}{2})/2T)}\right) \right]. \quad (2)$$

Based on the unit size and the epitaxial wafer structure, we obtain $a = 80 \mu\text{m}$, $L = 80 \mu\text{m}$ and $T = 8 \mu\text{m}$. Assuming that $I = 20 \text{ mA}$, we then obtain three possible values of w of $6 \mu\text{m}$, $10 \mu\text{m}$ and $20 \mu\text{m}$. The central current distribution of the active layer can then be calculated as shown in Fig. 3. Considering the fact that the opaque electrode has a light-shielding effect on the device, we must ensure that the electrode width is not too wide. As a result, we found that the square-circle electrode had an optimal width of $10 \mu\text{m}$.

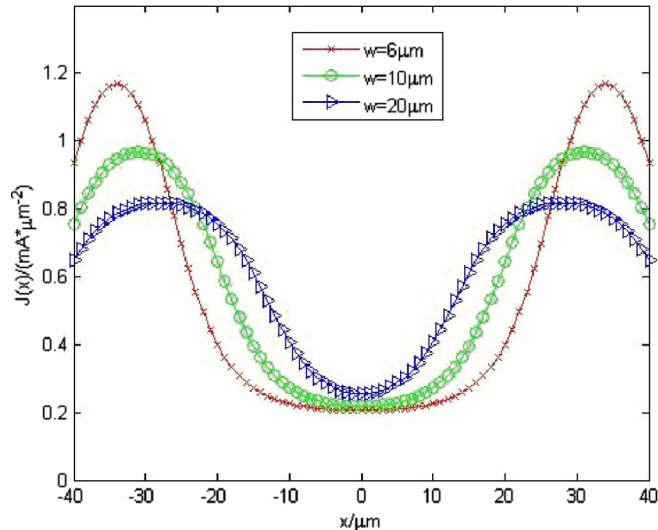


FIG. 3. Current density distributions on the active layer for various square-circle anode dimensions.

The internal quantum efficiency of the device can be calculated using Eq. (3):

$$\eta_{in} = \frac{R_r}{R_r + R_{nr}}, \quad (3)$$

where R_r is the radiative recombination rate and R_{nr} is the non-radiative recombination rate. Assuming that the concentrations of the electrons and the cavity in the junction are given by n and p , respectively, then the radiative recombination rate is given by the product Bnp , where B is the recombination coefficient, which was calculated to be $10^{-14} \text{ cm}^3/\text{s}$ at room temperature. The non-radiative processes include Shockley–Read–Hall recombination and Auger recombination, which could be represented by An , Cn^2p or Cnp^2 , where A and C are recombination coefficients. Because of the materials used in this study, A and C are $60 \text{ cm}^3/\text{s}$ and $10^{-31} \text{ cm}^3/\text{s}$, respectively, at room temperature. The internal quantum efficiency can then be rewritten using Eq. (4):

$$\eta_{in} = Bn^2/(An + Bn^2 + Cn^3). \quad (4)$$

The device current density is given by

$$j = ed(An + Bn^2 + Cn^3), \quad (5)$$

where e is the charge on a single electron and d is the active layer length, which is $1.1 \mu\text{m}$ in this device. From Eqs. (4) and (5), we obtain Eq. (6):

$$n = \frac{\sqrt[3]{s(j)}}{6C} + \frac{2B^2/3 - 2AC}{C\sqrt[3]{s(j)}} - \frac{B}{3C}, \quad (6)$$

where $s(j)$ is then given by Eq. (7):

$$s(j) = 36ABC - 8B^3 + 108C^2j + 12\sqrt{3}C\sqrt{4A^3C - A^2B^2 + (18ABC - 4B^3)j + 27C^2j^2}. \quad (7)$$

When the pn junction area is fixed, the relationship between the internal quantum efficiency and the anode current is the same as that between the internal quantum efficiency and the anode current density, as shown in Fig. 4.

As shown in Fig. 4, the current should be in the 0.42 – 1.06 mA range to guarantee that the internal quantum efficiency is higher than 85%. The corresponding voltage range is 2 – 2.3 V. We chose the driving voltage to be 2.2 V to obtain high internal quantum efficiency. The temperature distribution of the layers in a single unit was then simulated. As shown in Fig. 5, the maximum unit temperature

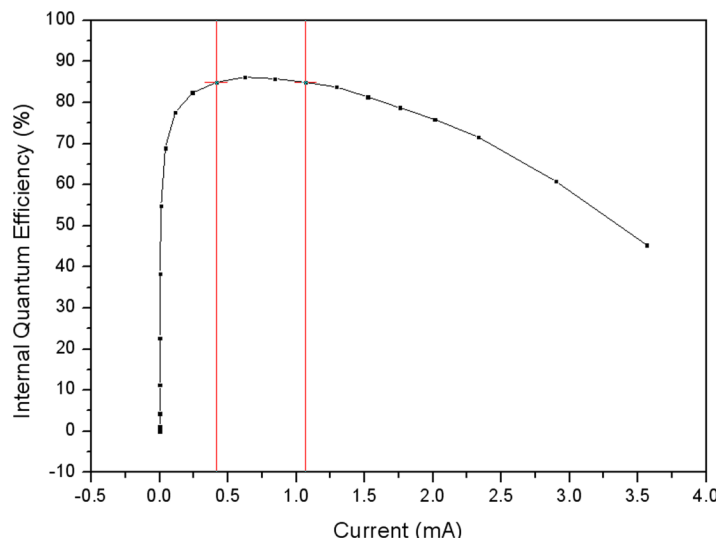


FIG. 4. Relationship between the internal quantum efficiency and the anode current.

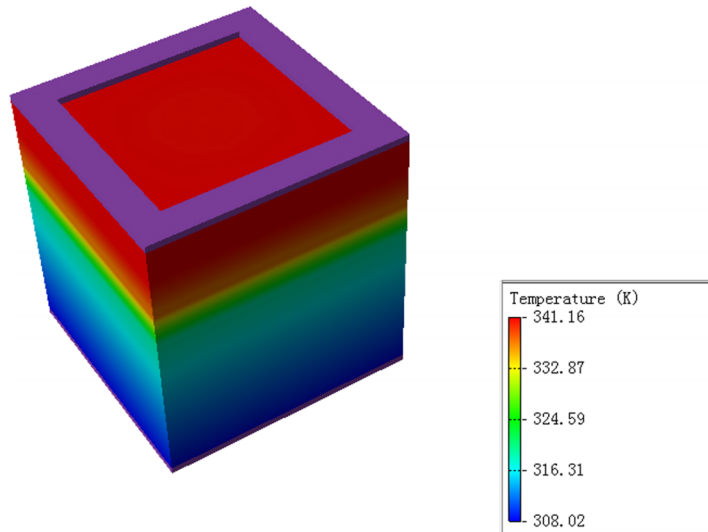


FIG. 5. Temperature distribution of the device layers.

was approximately 341 K, which can be reduced to a more reasonable value by using an appropriate heat-sink structure.¹⁶

DEVICE FABRICATION AND RESULTS

The MOEMS technology-based fabrication process of the AlGaInP micro-LEDs is shown in Figure 6.

- First, the isolation groove pattern was formed using SiO_2 , which was deposited by electron beam evaporation. The SiO_2 thickness was approximately 2 μm .
- The epitaxial wafer was then etched using an inductively coupled plasma (ICP) technique to expose the GaAs substrate underneath the LED units. The isolation groove was filled with insulating Si-polyurethane to block out the light.
- A patterned Ni/Au bilayer was then deposited on the p-GaP layer as a square-circle anode. This layer was then annealed to form stable ohmic contacts.
- The chip was packaged using epoxy resin to protect the surface from subsequent processing. The substrate was thinned by chemical etching to the bottom of the isolation groove so that adjacent units were completely isolated from each other.

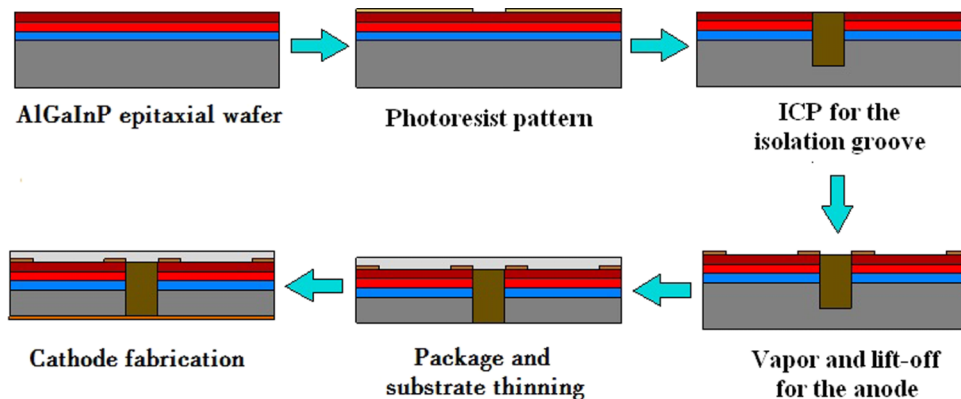


FIG. 6. Device fabrication process.

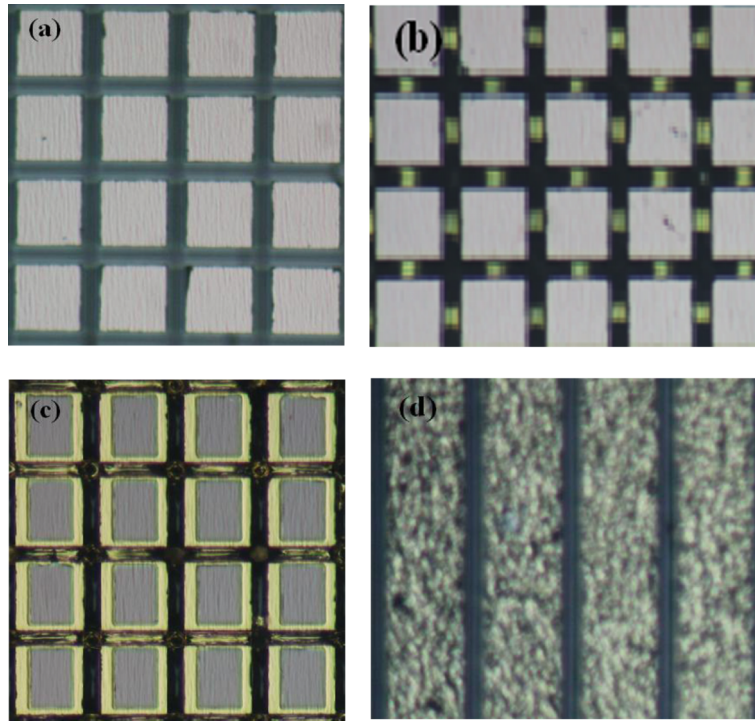


FIG. 7. Images of the AlGaInP-LED array during fabrication. (a) The array after ICP etching, (b) the micro-LED array with the insulated opaque medium, (c) the anodes of the array, and (d) the cathode of the arrays.

(e) Finally, Cr/Au layers were deposited by vapor deposition to act as a strip-shaped cathode. A lift-off process was then performed.

Figure 7 shows images of the device.

The I-V characteristics and the optical output power versus voltage curves of the micro-LEDs were measured. From the test results, we found from Figure 8 that the turn-on voltage of the LED microarray was 1.7 V, which was the same as that of the chip material itself; this occurred because the ideal ohmic contact electrode was used in the production process. The optical power output of a single pixel increased slightly with increasing current from 0 to 40 mA. The maximum optical power was 320 μ W when the current was 43 mA. Because the total input power is fixed, the Joule heat that was produced by each of the units will cause the light output power to decrease.

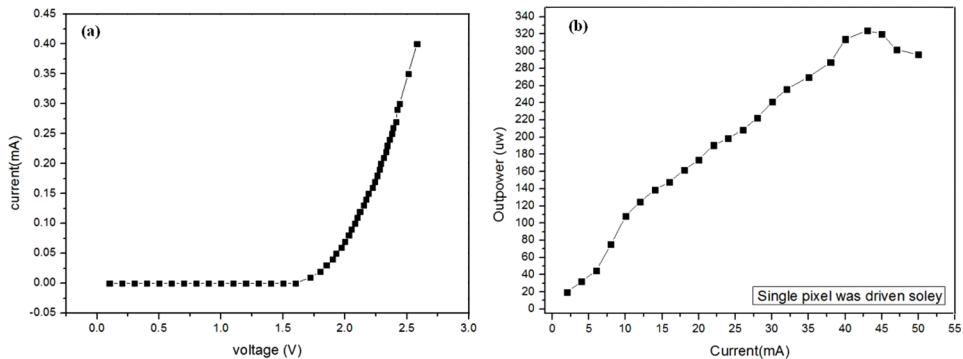


FIG. 8. Optical and electrical characteristics of the AlGaInP-LED array. (a) I-V characteristics of the micro-LEDs. (b) Optical output power versus voltage curves of the micro-LEDs.

CONCLUSION

An array of 320×240 micro-LEDs based on an AlGaInP epitaxial wafer with a unit size of $100 \mu\text{m} \times 100 \mu\text{m}$ was designed on the basis of a theoretical analysis. The width of the isolation groove between the adjacent light-emitting units was determined by the ratio of the emitting area to the area of each unit. Si-polyurethane composite was used to fill the groove, and could reflect part of the light from the sidewall toward the window layer to improve the light extraction efficiency. A square-circle anode with width of $10 \mu\text{m}$ was designed, and the results of simulations of the current and temperature distributions of the layers were shown. Finally, the device was fabricated using a MOEMS-based process. The device worked as expected. Through optimization of this process, we intend to improve the device parameters.

ACKNOWLEDGMENTS

This work was supported by the National Natural Science Foundation of China (NSFC) under grant no. 61274122, the Jilin Province Science and Technology Development Plan under grant nos. 20100351 and 20120323, and the Changchun Science and Technology Plan under grant no. 12ZX21.

- ¹ Y. C. Chu, M. H. Wu, C. J. Chung, Y. H. Fang, and Y. K. Su, *IEEE Electron Device Lett.* **35**, 771 (2014).
- ² J. Day, J. Li, D. Y. C. Lie, C. Bradford, J. Y. Lin, and H. X. Jiang, *Appl. Phys. Lett.* **99**, 031116 (2011).
- ³ H. X. Jiang and J. Y. Lin, *Opt. Express.* **21**, A475 (2013).
- ⁴ P. F. Tian, J. J. D. McKendry, Z. Gong, S. Zhang, S. Watson, D. D. Zhu, I. M. Watson, E. Gu, A. E. Kelly, C. J. Humphreys, and M. D. Dawson, *J. Appl. Phys.* **115**, 033112 (2014).
- ⁵ E. Matioli, S. Brinkley, K. M. Kelchner, Y. L. Hu, S. Nakamura, S. DenBaars, J. Speck, and C. Weisbuch, *Light: Science & Applications*, **1**, e22 (2012).
- ⁶ X. F. Li, J. D. Budai, F. Liu, J. Y. Howe, J. H. Zhang, X. J. Wang, Z. J. Gu, C. J. Sun, R. S. Meltzer, and Z. W. Pan, *Light: Science & Applications*, **2**, e50 (2013).
- ⁷ T. Liang, X. Guo, B. L. Guan, J. Guo, X. L. Gu, Q. M. Lin, and G. D. Shen, *Chin. Phys. Lett.* **24**, 1110 (2007).
- ⁸ S. C. Hsu, D. S. Wuu, X. H. Zheng, J. Y. Su, M. F. Kuo, P. Han, and R. H. Horng, *Semicond. Sci. Technol.* **23**, 105013 (2008).
- ⁹ Y. M. Song, E. S. Choi, J. S. Yu, and Y. T. Lee, *Opt. Express.* **17**, 20991 (2009).
- ¹⁰ J. W. Seo, H. S. Oh, J. S. Kwak, H. D. Song, K. W. Park, D. H. Park, S. W. Ryu, and Y. H. Park, *J. Korean Phys. Soc.* **55**, 314 (2009).
- ¹¹ T. Cheng, X. B. Luo, S. Y. Huang, and S. Liu, *Int. J. Therm. Sci.* **49**, 196 (2010).
- ¹² L. Kim, G. W. Lee, W. J. Hwang, J. S. Yang, and M. W. Shin, *Phys. Status Solidi C*, **7**, 2261 (2003).
- ¹³ M. S. Kim, H. K. Lee, and J. S. Yu, *Semicond. Sci. Technol.* **28**, 025005 (2013).
- ¹⁴ S. J. Chang, C. S. Chang, Y. K. Su, P. T. Chang, Y. R. Wu, K. H. Huang, and T. P. Chen, *IEEE Photon. Technol. Lett.* **9**, 182 (1997).
- ¹⁵ M. C. Amann and F. Kappeler, *Appl. Phys. Lett.* **48**, 1710 (1986).
- ¹⁶ N. C. Chen, Y. N. Wang, C. Y. Tseng, and Y. K. Yang, *Appl. Phys. Lett.* **89**, 101114 (2006).